Rietveld quantitative analysis of cast super duplex steel

J. L. Garin,[a] and R. L. Mannheim
Department of Metallurgical Engineering, Universidad de Santiago de Chile, Casilla 10233, Santiago, Chile

(Received 1 March 2012; accepted 14 March 2012)

To interpret highly superimposed diffraction patterns, the Rietveld method together with conventional X-ray powder diffraction techniques were carried out on a series of heat-treated weldments of cast super duplex stainless steel. High temperature processing of this type of alloys causes embrittlement and loss of corrosion resistance owing to precipitation of intermediate phases, principally sigma-phase. The annealing processing of the samples proceeded at temperatures in the range of 800–950 °C for periods of time from 1 to 96 h. This procedure permitted an accurate quantification of the microstructural components such as austenite, ferrite and sigma-phase in all studied samples. The contents of sigma-phase in the heat-affected zones of all weldments reached asymptotical values of 30–38 wt% after 96 h of heat treatment. © *International Centre for Diffraction Data*
[doi:10.1017/S0885715612000383]

Key words: Rietveld refinement, X-ray diffraction, super duplex steel, sigma phase

I. INTRODUCTION

A number of high-alloy stainless steels, usually known as duplex stainless steels (DSS), are an important class of engineering materials currently being considered for a variety of heavy-service requirements, among many industrial applications (Noble, 1993; Gunn, 1997). In fact, the widespread application of duplex steels is based on their remarkable mechanical and chemical properties such as strength (Liou *et al.*, 2001), chloride stress-corrosion cracking-resistance (Yang and Castle, 2002) and pitting corrosion-resistance (Cvijovic and Radenkovic, 2006). DSS are two-phase alloys based on the Fe–Cr–Ni system. They have approximately equal proportions of the body-centred cubic ferrite and face-centred cubic austenite phases in their microstructure. These materials are further characterized by their very low carbon content (<0.03%) and additions of molybdenum, nitrogen, tungsten and copper. The usual contents of chromium and nickel are in the range of 20–30% for Cr and 5–10% for Ni. To determine the extent of pitting corrosion resistance offered by the material, the pitting resistance equivalent (PRE) is commonly used (Herbsleb, 1982). A minimum PRE value of 40 is often used to define the super grades. Among the many manufacturing processes involving wrought and cast DSS, welding metallurgy plays a key role (Badji *et al.*, 2008). However, the performance of DSS can be significantly affected by the welding process (El Koussy *et al.*, 2004). Hence, the high alloy content and the presence of a ferritic matrix renders DSS susceptible to embrittlement, loss of mechanical properties and corrosion resistance when the material is subjected to relatively high temperatures, e.g. 540–900 °C (Pohl *et al.*, 2007). This is caused by the transformation of the ferritic component into the so-called sigma-phase (σ) (Pohl and Stortz, 2004). This phase is a complex intermetallic compound of Fe, Cr and, to a lesser extent, Mo (Sopousek and Kruml, 1996). The structure type of the compound is based on an ideal stoichiometric composition AX_2, Pearson codes tP30 and space group $P4_2/mnm$ (Sihna, 1972). Since the chemical composition of the compound in the Fe–Cr system is approximately Cr_6Fe_7, the Cr and Fe atoms are disordered with fractional site occupation among the suitable equivalent positions in the space group, disclosing a polyhedral array of the Frank–Kasper type (Pearson, 1972). Sigma preferably nucleates along grain boundaries of δ-ferrite–austenite, α-ferrite–austenite or δ-ferrite–δ-ferrite. Compounds with nearly equi-atomic composition in Fe and Cr are formed by an order–disorder transformation of the ferrite phase, whereas those with a smaller content of Cr precipitate through a eutectoid transformation of the kind $\alpha = \gamma + \sigma$, with γ being called secondary austenite (Tseng *et al.*, 1994).

Owing to the highly detrimental effects of sigma-phase precipitation on the mechanical and chemical properties of the DSS alloys, the determination of relative amounts in the microstructure by means of quantitative X-ray diffraction demands a rather precise processing of the experimental data. Taking into account the usually complex powder diffraction patterns of these alloys, which disclose many overlapping reflections, and the strong preferred orientations of the matrix components caused by solidification dendrites formed in castings as well as in welded joints, the present article describes the application of the Rietveld method to resolve the referred difficulties in weldments of a super duplex stainless steels subjected to annealing at various temperatures and processing times.

II. EXPERIMENTAL

A. Samples preparation

The raw alloy utilized in the present study was supplied on demand by a commercial steel producer. All casts were poured in the classical Y-shape moulds, according to ASTM A395 standard, to deliver samples of 50 mm thickness. The average chemical composition of the resulting Y-shaped ingots, determined by means of emission spectroscopy, is detailed in Table I. The contents of the main elements are within the composition ranges defined by ASTM A 890/A 890 M standard (UNS J93404).

Specimens suitable for heat treatment, light microscopy and X-ray powder diffraction experiments, of dimensions

[a]Author to whom correspondence should be addressed. Electronic mail: jorge.garin@usach.cl

TABLE I. Chemical composition of the cast alloy (mass %).

Element	Sample	Standard
C	0.026	0.03 max
Si	0.56	1.00 max
Mn	0.90	1.50 max
P	0.01	0.04 max
S	0.001	0.04 max
Cr	24.77	24.0–26.0
Ni	6.41	6.0–8.0
Mo	3.94	4.0–5.0
N	0.25	0.10–0.30

45 mm × 25 mm × 5 mm were machined from the test section of the Y-blocks. Observation surfaces were prepared by usual metallographic techniques, up to a final step of wet polishing with alumina of 0.05 μm particle size. The manufacturing of the weldments (butt joints with "X" bevels) was carried out by means of the usual manual arc welding technology [shielded metal arc welding (SMAW)] with INOX 2509MoB electrode. The heat treatment process included 1 h homogenization annealing at 1050 °C followed by heating for sigma-phase induction at 800, 860, 900 and 950 °C, for various periods of time from 1 to 96 h.

B. X-ray diffraction measurements

The X-ray powder diffraction data were collected at room temperature (24 °C) on a SIEMENS D5000 diffractometer (40 kV, 30 mA) equipped with a diffracted-beam graphite monochromator, Cu $K\alpha$ radiation ($\lambda_{K\alpha1} = 0.15406$ nm, $\lambda_{K\alpha2} = 0.15444$ nm, $I_{K\alpha1}/I_{K\alpha2} = 0.5$), Bragg–Brentano geometry, θ–θ scan, sample spinning (15 RPM), divergence slit of 1 mm, anti-scatter slit of 1 mm and receiving slit of 0.1 mm. The X-ray diffraction measurements were carried out within the scan range of 30°–85° 2θ with step size of 0.02° 2θ and step counting time of 15 s.

III. RESULTS AND DISCUSSION

Owing to the extensive number of processed samples, the experimental results are now described in terms of representative samples of the raw alloy and weldments annealed at selected temperatures for 3, 6, 12, 24, 48, 72 and 96 h. The light-microscopy metallography shows the morphology and particle size distribution of the diffracting surfaces of the specimens. Hence, Figure 1 reveals the microstructure of the as-cast material, where a distribution of irregular-shape austenite grains (light particles) is superimposed on a matrix of ferrite (dark background). Figure 2 illustrates the precipitation of sigma-phase in the heat-affected zone (HAZ) of the weldment annealed at 900 °C during 72 h. As depicted in the micrograph, sigma particles were brought in dark brown tones after etching with the proper reagent. Here, a massive distribution of small sigma particles is encountered along the austenite–austenite grain boundaries, where nucleation preferably takes place. The formation of sigma-phase with longer treatment times shows much thicker particles, distributed along ferrite–ferrite boundaries. This clearly indicates that particles originally nucleated along grain boundaries grew towards the ferritic phase, increasing their relative presence in the alloy, while the content of ferrite was conversely diminished. Next, a qualitative identification by X-ray powder diffraction was performed on all studied samples. Hence, ternary ferrite (Fe–Cr–Ni) and ternary austenite (Fe–Cr–Ni) were found in the parent alloy, in close agreement with the pattern shown in Figure 3. According to this diffraction pattern, formation of sigma-phase does not occur in this kind of specimens. Furthermore, the pattern evidences strong preferred orientation effects of the (200) lattice planes in the ferrite solid solution phase. Figures 4–10 show the XRD patterns of samples corresponding to the annealed weldments at 860 °C for 3, 6, 12, 24, 48, 72 and 96 h, respectively.

Formation of sigma as well as significant preferred orientations of the component phases can be corroborated in all heat-treated samples. To determine the relative amount of phases in the heat-treated alloys, particularly sigma-phase, quantitative X-ray powder diffraction based on the Rietveld processing of the data (McCusker *et al.*, 1999), was performed on all samples. The refinements were carried out assuming the split Pearson VII function for the simulation of the peaks

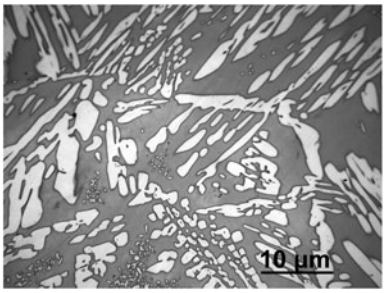

Figure 1. Microstructure of the as-cast alloy.

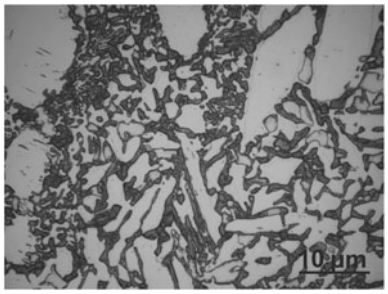

Figure 2. Microstructure of the weldment (HAZ) annealed at 860 °C for 72 h.

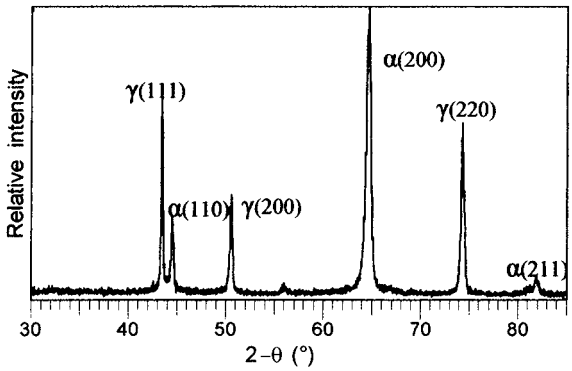

Figure 3. XRD pattern of parent alloy (γ, austenite; α, ferrite).

https://doi.org/10.1017/S0885715612000383 Published online by Cambridge University Press

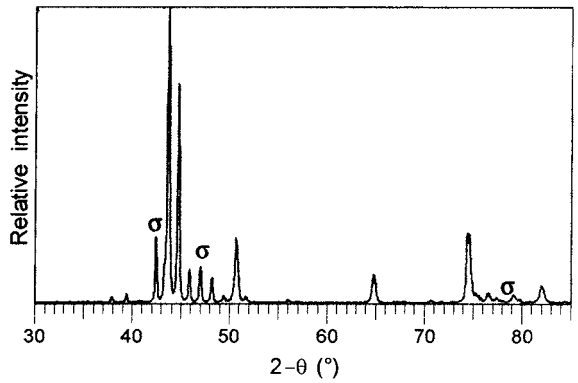

Figure 4. XRD pattern of weldment (HAZ) annealed at 860 °C for 3 h.

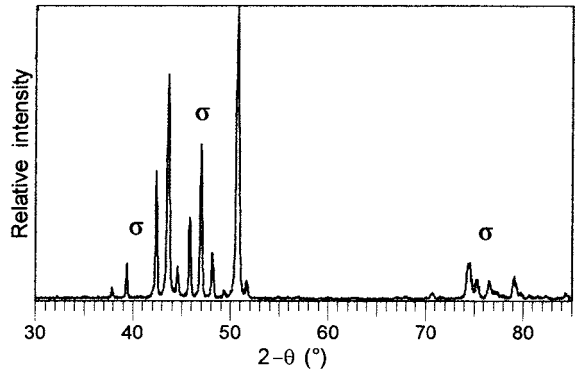

Figure 5. XRD pattern of weldment (HAZ) annealed at 860 °C for 6 h.

shape, while the background was modelled by a fourth-order Chebychev polynomial; the refinement cycles were based on the variation of structural and instrumental parameters. The correction term for the presence of textures utilized the March–Dollase function (Dollase, 1986), represented by

$$P_K = \left(G_1^2 \cos^2 \alpha + \left(1/G_1\right) \sin^2 \alpha\right)^{-3/2}, \quad (1)$$

where α is the angle between the normal to the diffracting plane and the presumed cylindrical-symmetry axis of the texture and G_1 is a numerical refinable parameter. Owing to the somewhat simple formation of dendrites in the weldments, the uniaxial March–Dollase model is applicable to welded specimens of duplex stainless steels. The crystal data utilized

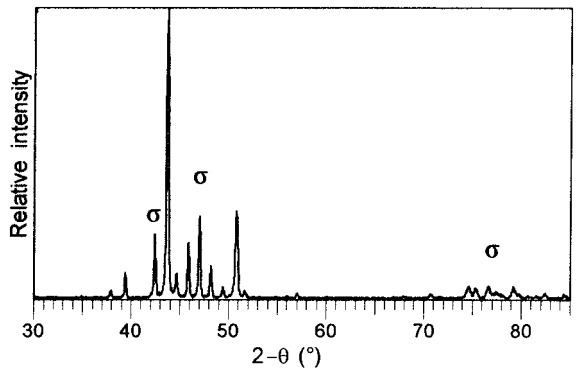

Figure 6. XRD pattern of weldment (HAZ) annealed at 860 °C for 12 h.

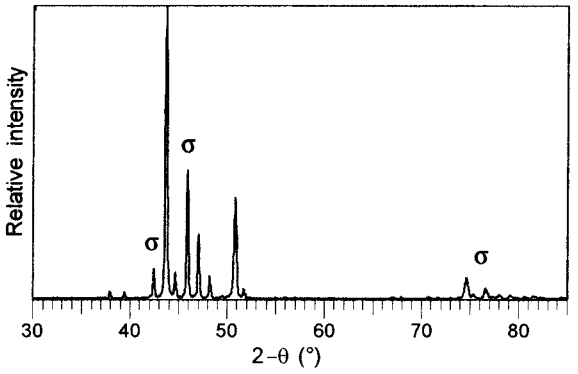

Figure 7. XRD pattern of weldment (HAZ) annealed at 860 °C for 24 h.

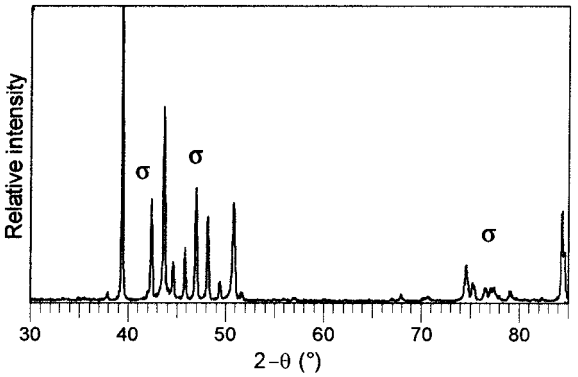

Figure 8. XRD pattern of weldment (HAZ) annealed at 860 °C for 48 h.

in the calculation of the structure factors were those reported from single-crystal analysis of sigma-phase (Yaquel, 1983a, 1983b), detailed in Table II. The relative amount of phases was calculated by means of the equation (Hill, 1991):

$$W_{\mathrm{p}} = \frac{S_{\mathrm{p}}(\mathrm{ZM}V)_{\mathrm{p}}}{\sum_{i=1}^{N} S_i(\mathrm{ZM}V)_i}, \quad (2)$$

where W_{p} is the mass concentration of phase p, S_{P} is the scale factor of phase p, ZM is the molecular weight of the unit cell, V is the volume of the unit cell and N is the number of crystalline phases in the specimen. The Rietveld code used was the DBWS-9807a system of programs (Young *et al.*, 1999). The numerical results obtained by the application of the described

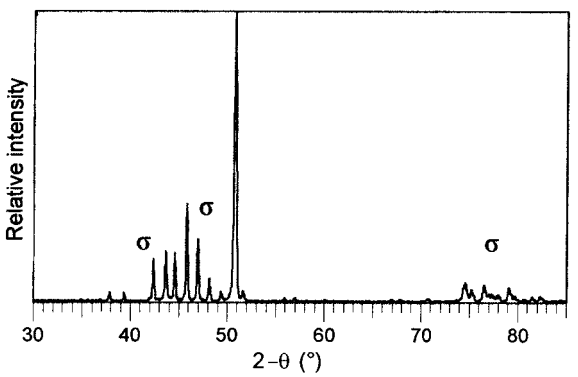

Figure 9. XRD pattern of weldment (HAZ) annealed at 860 °C for 72 h.

https://doi.org/10.1017/S0885715612000383 Published online by Cambridge University Press

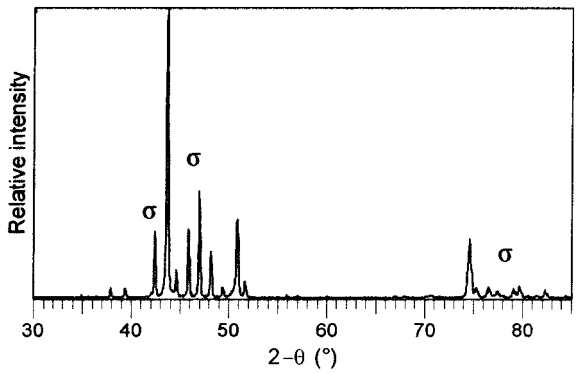

Figure 10. XRD pattern of weldment (HAZ) annealed at 860 °C for 96 h.

TABLE II. Crystal data for sigma-phase.

Unit formula	Cr_6Fe_7
Pearson symbol	*tP*30
Structure type	$D8_b$ (Cr_6Fe_7)
Space group	$P4_2/mnm$
Unit cell parameters (Å)	$a = 8.785$
	$c = 4.579$
Volume (Å^3)	353.39
Z	10
M (g mol^{-1})	702.95
D_x/Mg m^{-3}	7.63
Atom positions in space group	0.75Cr + 0.25Fe 4g
	0.66Cr + 0.34Fe 8*j*
	0.62Cr + 0.34Fe 8*i*
	0.16Cr + 0.84Fe 8*i*
	0.12Cr + 0.88Fe 2*a*

procedure to a metallurgical problem, are graphically represented in Figures 11 and 12. It can be observed that the fraction of precipitated particles of sigma increases with heating time at a given temperature, resembling the well-known mechanism of Johnson–Mehl–Avrami (Cahn and Haasen, 1996), based on the nucleation and growth phenomenon in metals and alloys, as described by Eq. (3):

$$X_\sigma = a[1 - \exp(-kt^n)], \quad (3)$$

where X_σ is the fraction of precipitated sigma-phase, which

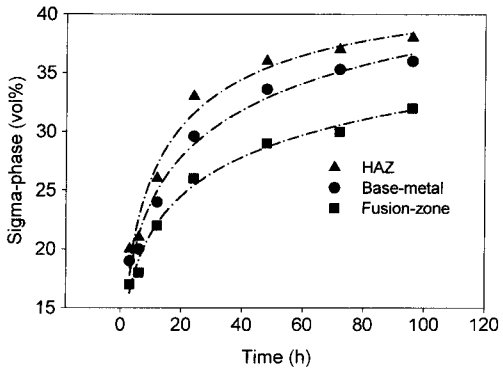

Figure 11. Relative amount of sigma-phase vs. annealing time of the weldment.

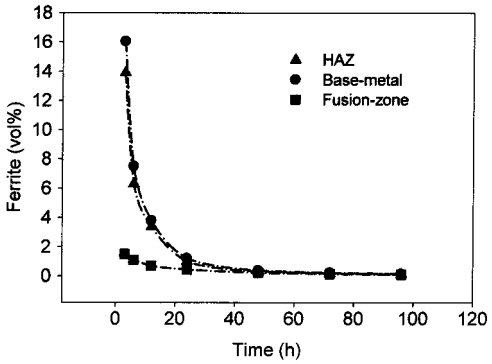

Figure 12. Relative amount of ferrite vs. annealing time of the weldment.

nucleates and grows from ferrite particles, *t* is the transformation time and *a*, *k* and *n* are transformation parameters.

IV. CONCLUSION

In summary, we have assessed the application of the Rietveld method to quantify the formation of sigma-phase in weldments of duplex stainless steels subjected to annealing at relatively high temperatures. The main advantage of this methodology was the use of the March–Dollase model for correction of the strong texture effects on the diffraction pattern, which yielded the lower *R*-values and much better represented the relative amounts of phases in the samples. In fact, the alternative technique of computer-aided microscopy, where image analysis depends greatly upon the ability of the optical system to resolve the subject, generally yields poor-quality data when more than two phases are involved. From the metallurgical point of view, the results of XRD followed by Rietveld analysis indicated that the larger the annealing time of the welded parts, the larger will be the volume fraction of the precipitated particles of the intermediate phase, in good agreement with the Johnson–Mehl–Avrami relationship. Furthermore, sigma particles nucleate and grow reaching saturation levels depending on the specific type of alloy.

ACKNOWLEDGEMENTS

This work was supported by Universidad de Santiago de Chile (USACH) and the Chilean Research Funding Agency (FONDECYT Project No. 1085053). We greatly appreciate these financial assistances, as well as experimental assistance provided by Mrs Alicia Duran, Ms Gladys Olivares and Mr Felipe Gutiérrez, from the Department of Metallurgical Engineering.

Badji, R., Bouabdallah, M., Bacroix, B., Kahloun, C., Bettahar, K., and Kherrouba, N. (**2008**). "Phase transformation and mechanical behaviour in annealed 2205 duplex stainless steel welds," Mater. Charact. **59**, 447–453.

Cahn, R. W. and Haasen, P. (**1996**). *Physical Metallurgy* (North Holland, Amsterdam).

Cvijovic, Z. and Radenkovic, G. (**2006**). "Microstructure and pitting corrosion resistance of annealed duplex stainless steel," Corros. Sci. **48**, 3887–3906.

Dollase, W. A. (**1986**). "Correction of intensities for preferred orientation in powder diffractometry: application of the March model," J. Appl. Crystallogr. **19**, 267–272.

El Koussy, M., El Mahallawi, I. S., Califa, W. E., Al Dawood, M., and Bueckins, M. (**2004**). "Effects of thermal aging on microstructure and

https://doi.org/10.1017/S0885715612000383 Published online by Cambridge University Press

mechanical properties of duplex stainless steel weldments," Mater. Sci. Technol. **20**, 375–381.
Gunn R. N. (Ed.) (**1997**). *Duplex Stainless Steels, Microstructure, Properties and Applications* (Abington, Cambridge).
Herbsleb, G. (**1982**). "The influence of SO_2, H_2S and CO on pitting corrosion of austenitic chromium-nickel stainless steels with up to 4 wt.% molybdenum in 1 M NaCl," Werkst. Korros. **33**, 334–340.
Hill, R. J. (**1991**). "Expanded use of the Rietveld method in studies of phase abundance in multiphase mixtures," Powder Diffr. **6**, 1615–1631.
Liou, H., Pan, Y., Hsieh, R., and Tsai, W. (**2001**). "Effects of alloying elements on the mechanical properties and corrosion behaviour of 2205 duplex stainless steel," J. Mater. Eng. Perf. **10**, 231–241.
McCusker, L. B., Von Reele, R. B., Cox, D. E., Louer, D., and Scardi, P. (**1999**). "Rietveld refinement guidelines," J. Appl. Crystallogr. **32**, 36–50.
Noble, D. N. (**1994**). "Selection of wrought duplex stainless steels," in *Stainless Steels, Specialty Handbook*, edited by J. R. Davis (American Society for Metals, Metals Park) pp. 471–481.
Pearson, W. B. (**1972**). *The Crystal Chemistry and Physics of Metals and Alloys* (Willey, New York).
Pohl, M. and Stortz, O. (**2004**). "Sigma-phase in duplex stainless steels," Z. Metallkd. **95**, 631–638.
Pohl, M., Stortz, O., and Glogowski, T. (**2007**). "Effect of intermetallic precipitation on the properties of duplex stainless steel," Mater. Charact. **58**, 65–71.
Sihna, A. K. (**1972**). "Topologically close-packed structures of transition metal alloys," Mater. Sci. **15**, 104–109.
Sopousek, J. and Kruml, T. (**1996**). "Sigma-phase equilibria and nucleation in Fe–Cr–Ni alloys at high temperature," Scr. Mater. **35**, 689–693.
Tseng, C., Thompson, S., Mataya, M., and Krauss, G. (**1994**). "Fracture and the formation of sigma-phase, $M_{23}C_6$, and austenite from delta-ferrite in an AISI stainless steel," Metall. Trans., Sect. A; Phys. Metall. Mater. Sci. **25**, 1147–1158.
Yaquel, H. L. (**1983a**). "Atom distributions in sigma phases. I. Fe and Cr atom distributions in a binary sigma-phase equilibrated at 1063 and 923K," Acta Crystallogr., Sect. B: Struct. Sci. **29**, 20–28.
Yaquel, H. L. (**1983b**). "Atom distributions in sigma phases. II. Estimation of average site-occupation parameters in a sigma phase containing Fe, Cr, Ni, Mo and Mn," Acta Crystallogr., Sect. B: Struct. Sci. **29**, 28–33.
Yang, R. A., Larson, A. C., and Paiva-Santos, C. O. (**1999**). *Rietveld Analysis of X-rays and neutron Diffraction Patterns* (Georgia Institute of Technology, Atlanta).
Yang, X. F. and Castle, J. E. (**2002**). "Using *in situ* AFM to investigate corrosion and passivation of duplex stainless steels," Surf. Interface Anal. **33**, 894–899.